



CHALMERS
UNIVERSITY OF TECHNOLOGY

Regulation of yeast-to-hyphae transition in *Yarrowia lipolytica*

Downloaded from: <https://research.chalmers.se>, 2024-04-23 14:37 UTC



Citation for the original published paper (version of record):

Pomraning, K., Bredeweg, E., Kerkhoven, E. et al (2018). Regulation of yeast-to-hyphae transition in *Yarrowia lipolytica*. *mSphere*, 3(6). <http://dx.doi.org/10.1128/mSphere.00541-18>

N.B. When citing this work, cite the original published paper.



Regulation of Yeast-to-Hyphae Transition in *Yarrowia lipolytica*

Kyle R. Pomraning,^a Erin L. Bredeweg,^b Eduard J. Kerkhoven,^c Kerrie Barry,^d Sajeet Haridas,^d Hope Hundley,^d Kurt LaButti,^d Anna Lipzen,^d Mi Yan,^d Jon K. Magnuson,^{a,e} Blake A. Simmons,^e Igor V. Grigoriev,^d  Jens Nielsen,^{c,f}  Scott E. Baker^{b,e}

^aChemical & Biological Process Development Group, Pacific Northwest National Laboratory, Richland, Washington, USA

^bEnvironmental Molecular Sciences Division, Pacific Northwest National Laboratory, Richland, Washington, USA

^cDepartment of Biology and Biological Engineering, Chalmers University of Technology, Göteborg, Sweden

^dDOE Joint Genome Institute, Walnut Creek, California, USA

^eJoint BioEnergy Institute, Lawrence Berkeley National Laboratory, Berkeley, California, USA

^fNovo Nordisk Foundation Center for Biosustainability, Technical University of Denmark, Lyngby, Denmark

ABSTRACT The yeast *Yarrowia lipolytica* undergoes a morphological transition from yeast-to-hyphal growth in response to environmental conditions. A forward genetic screen was used to identify mutants that reliably remain in the yeast phase, which were then assessed by whole-genome sequencing. All the *smooth* mutants identified, so named because of their colony morphology, exhibit independent loss of DNA at a repetitive locus made up of interspersed ribosomal DNA and short 10- to 40-mer telomere-like repeats. The loss of repetitive DNA is associated with down-regulation of genes with stress response elements (5'-CCCCT-3') and upregulation of genes with cell cycle box (5'-ACGCG-3') motifs in their promoter region. The stress response element is bound by the transcription factor Msn2p in *Saccharomyces cerevisiae*. We confirmed that the *Y. lipolytica* *msn2* (*Ylmsn2*) ortholog is required for hyphal growth and found that overexpression of *Ylmsn2* enables hyphal growth in *smooth* strains. The cell cycle box is bound by the Mbp1p/Swi6p complex in *S. cerevisiae* to regulate G₁-to-S phase progression. We found that overexpression of either the *Ylmbp1* or *Ylswi6* homologs decreased hyphal growth and that deletion of either *Ylmbp1* or *Ylswi6* promotes hyphal growth in *smooth* strains. A second forward genetic screen for reversion to hyphal growth was performed with the *smooth-33* mutant to identify additional genetic factors regulating hyphal growth in *Y. lipolytica*. Thirteen of the mutants sequenced from this screen had coding mutations in five kinases, including the histidine kinases *Ylchk1* and *Ylnik1* and kinases of the high-osmolarity glycerol response (HOG) mitogen-activated protein (MAP) kinase cascade *Ylssk2*, *Ylpbs2*, and *Ylhog1*. Together, these results demonstrate that *Y. lipolytica* transitions to hyphal growth in response to stress through multiple signaling pathways.

IMPORTANCE Many yeasts undergo a morphological transition from yeast-to-hyphal growth in response to environmental conditions. We used forward and reverse genetic techniques to identify genes regulating this transition in *Yarrowia lipolytica*. We confirmed that the transcription factor *Ylmsn2* is required for the transition to hyphal growth and found that signaling by the histidine kinases *Ylchk1* and *Ylnik1* as well as the MAP kinases of the HOG pathway (*Ylssk2*, *Ylpbs2*, and *Ylhog1*) regulates the transition to hyphal growth. These results suggest that *Y. lipolytica* transitions to hyphal growth in response to stress through multiple kinase pathways. Intriguingly, we found that a repetitive portion of the genome containing telomere-like and rDNA repeats may be involved in the transition to hyphal growth, suggesting a link between this region and the general stress response.

Received 3 October 2018 Accepted 26 October 2018 Published 5 December 2018

Citation Pomraning KR, Bredeweg EL, Kerkhoven EJ, Barry K, Haridas S, Hundley H, LaButti K, Lipzen A, Yan M, Magnuson JK, Simmons BA, Grigoriev IV, Nielsen J, Baker SE. 2018. Regulation of yeast-to-hyphae transition in *Yarrowia lipolytica*. mSphere 3:e00541-18. <https://doi.org/10.1128/mSphere.00541-18>.

Editor Aaron P. Mitchell, Carnegie Mellon University

Copyright © 2018 Pomraning et al. This is an open-access article distributed under the terms of the [Creative Commons Attribution 4.0 International license](#).

Address correspondence to Kyle R. Pomraning, kyle.pomraning@pnnl.gov, or Scott E. Baker, scott.baker@pnnl.gov.

KEYWORDS *Yarrowia*, dimorphic, genomics, molecular genetics, morphology, signaling

Many fungi harbor the ability to grow in either a yeast, pseudohyphal, or hyphal form (1). Morphological plasticity allows fungi to adapt to and invade new environments in response to external conditions. This trait, while essential for fungi in natural environments, can be problematic for their use in industrial settings, such as cultivation in bioreactors. The morphological switch between yeast and hyphal growth can be initiated by nutritional, pH, temperature, and osmolarity cues (2–5). Industrial utilization of dimorphic yeasts presents a particular challenge, as maximum economic efficiency demands that bioreactors be run at high temperature and osmolarity using low-quality nutrients, all of which may initiate the switch to hyphal growth.

Dimorphism is common in many species of ascomycete yeasts and has been most thoroughly studied in the genetic model *Saccharomyces cerevisiae* and the closely related opportunistic pathogen *Candida albicans* where the switch to hyphal growth is important for infection (6). Environmental signals controlling hyphal growth regulate specific genetic outputs through kinase cascades and calcium signaling pathways. The adenylate cyclase Cyr1p is required for hyphal growth in yeasts (7, 8) and signals through protein kinase A (PKA) to the transcription factor Efg1p to promote the yeast-to-hyphae transition (9, 10). Two mitogen-activated protein kinase (MAPK) cascades integrate signals from different sources to position and regulate filamentous growth in yeasts. The kinase Ste20p responds to the GTPase Cdc42p and activates the Ste11p/Ste7p/Kss1p MAPK cascade to control polarized growth and bud site selection (5, 11, 12), while the Ssk2p/Pbs2p/Hog1p MAPK cascade responds to osmotic and oxidative stress in *S. cerevisiae* and *C. albicans* and regulates the yeast-to-hyphae transition in both species (10, 13, 14).

Yarrowia lipolytica is a model industrial ascomycete yeast distantly related to *S. cerevisiae* and *C. albicans* (15). The yeast-to-hyphae transition in this species has been examined by proteomics and transcriptomics (16, 17) and has given clues to the proteins involved. The transition is regulated by a number of transcription factors, including those encoded by *znc1* (18), *tec1* (19), *hoy1* (20), and the histone deacetylase complex component gene *sin3* (21). The *Y. lipolytica* *msn2* (*Ylmsn2*) homolog (originally identified as *mhy1* in *Y. lipolytica*) is critical for the yeast-to-hyphae transition and is positively regulated by the kinase Rim15p which itself is repressed by the Tor nitrogen signaling pathway (22, 23). As in other yeasts, Ras GTPases (Ras1p and Ras2p) are essential for the dimorphic transition and also likely signal through the transcription factor Msn2p (24, 25).

In this study, we isolated strains of *Y. lipolytica* that fail to undergo the yeast-to-hyphae transition. These *smooth* colony mutants do not form hyphae in a bioreactor, making them more amenable as industrial bioproduction hosts. We characterized the mutations present in the mutants obtained and mutations that promote the transition to hyphal growth in a *smooth* strain to further elucidate the signaling pathways regulating dimorphic growth in *Y. lipolytica*.

RESULTS

Isolation of *Y. lipolytica* mutants lacking filamentous growth. *Y. lipolytica* strain FKP355 was passaged to allow accumulation of mutations and screened for lack of filamentous growth from large colonies. Small slow growing colonies often did not produce hyphae or did so only under certain conditions or after an extended period of time. Approximately 500,000 colonies were screened from which 65 mutants were isolated that did not appear to make hyphae. After isolation, these mutants were further tested for filamentous growth after 2 weeks of incubation on YNB, YNB150, and YPD agar (see Materials and Methods), as well as YPD and YNB150 liquid medium for microscopic analysis. From those mutants, five *smooth* mutants (*smooth-17*, *smooth-18*, *smooth-19*, *smooth-33*, and *smooth-43*) were identified that did not undergo transition

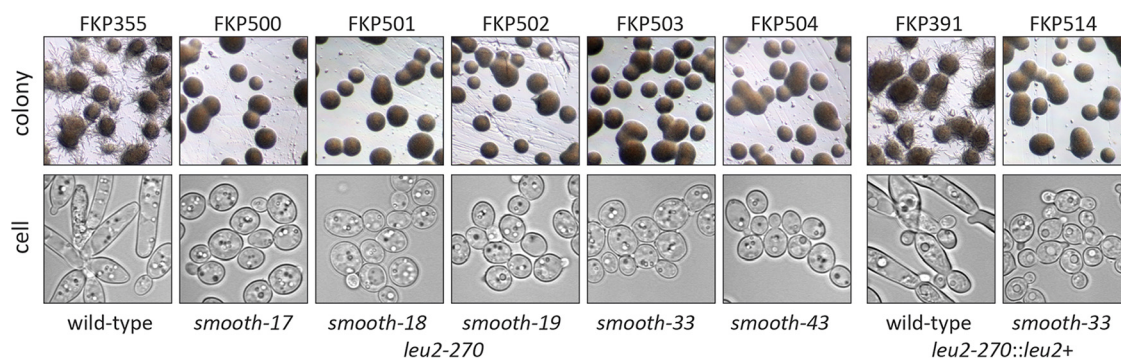


FIG 1 Isolation of *Y. lipolytica* mutants that lack filamentous growth. Approximately 500,000 colonies were screened for *smooth* morphology with no visible hyphae. From strain FKP355, five mutant strains were isolated that exhibit growth only as yeast (FKP500 to FKP504). The *leu2-270* mutation was complemented in strain FKP503 to construct FKP514 and confirm the phenotype in a prototrophic strain. Confocal microscopy confirmed yeast phase growth and lack of elongated cells or pseudohyphae in auxotrophic and prototrophic *smooth* strains.

to hyphal growth morphology under any of the conditions tested (Fig. 1). Many of the original 65 isolates produced short invasive hyphae into the agar or grew slowly and were not considered further in this work. Approximately 100,000 colonies from each of the five mutants were screened for reversion to hyphal growth habit from the *smooth* phenotype. No revertants ($<0.0002\%$) from any of the mutants were identified, confirming genetic stability.

Identification of mutations in *Y. lipolytica* mutants lacking filamentous growth.

Each of the five mutants lacking filamentous growth and the wild-type parent (FKP355) were sequenced using Illumina paired-end 150-base-pair sequencing to an average depth of $>13\times$ to identify the causative mutations. This initial search revealed few mutations limited to a single nucleotide polymorphism (SNP) affecting a tRNA in *smooth-17*, a deletion in gene Yali0F20592g in *smooth-19*, and a noncoding SNP in *smooth-43*. None of these candidate genes complemented the *smooth* phenotype when expressed from an autonomously replicating plasmid (data not shown). To better assess the mutants, genomic DNA from strain FKP355 was sequenced on the PacBio platform to a depth of $279\times$, assembly and annotation of which are available at <http://genome.jgi.doe.gov/Yarlip1/Yarlip1.info.html>. Using this assembled genome allowed us to search for gaps in read coverage in the mutants and resulted in identification of deletions in *smooth-17*, *smooth-33*, and *smooth-43* strains. Interestingly, the deletions are in the same general location near the end of scaffold 14 in all three of these *smooth* mutants (Fig. 2A). Analysis of the mutated region of scaffold 14 revealed that it ends in an array of polymorphic 5'-TTAGTCAGGG-3' tandem DNA repeats previously described as the telomere repeat sequence in *Y. lipolytica* (26). Exceptionally high sequencing read depth at this locus suggests that it is highly repetitive and underrepresented in the genome assembly. We therefore sought to explore the possibility of alternative assemblies of the DNA at the end of scaffold 14 to better understand the composition of this mutated locus.

We hypothesized that the length of the repetitive DNA present at the end of scaffold 14 is much longer than the ~ 800 bp represented in the genome assembly and used long PacBio sequencing reads from strain FKP355 to test this. We identified 3,786 reads ranging from 117 to 29,910 bp in length (average of 3,548 and median of 2,331 bp) that aligned to a unique portion of the genome near the end of scaffold 14. This subset of reads was assembled using Canu (27) to assess the minimum length and content of the repetitive DNA adjacent to the end of the unique part of scaffold 14 without assembly interference from additional repetitive reads from different loci. From these reads, seven alternative contigs to scaffold 14 were assembled that mapped to a variety of scaffolds within the reference genome, confirming the repetitive nature of the locus. We aligned the 150-bp Illumina sequencing reads from strain FKP355 and the five *smooth* mutants to these new contigs and identified mutations. Interestingly, six out of

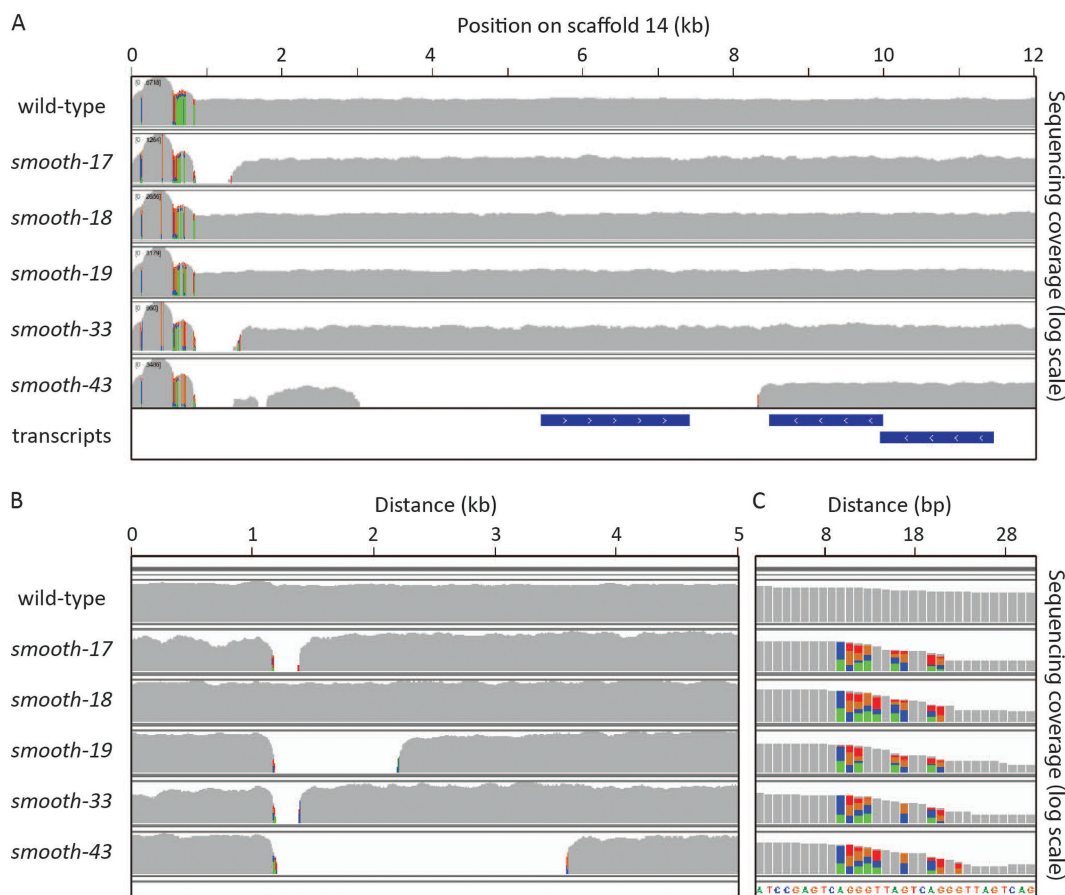


FIG 2 *smooth* strains have mutations in repetitive regions of the genome. Coverage from high-throughput 150-bp paired-end Illumina sequencing from strain FKP355 (wild type) and five *smooth* mutant strains. Colored bases indicate polymorphic loci where reads align with SNPs at a rate greater than that expected from incorrect base calls. (A) Regions with no coverage are detected in *smooth-17*, *smooth-33*, and *smooth-43* mutants at the end of scaffold 14 after alignment to the FKP355 reference genome. (B) Raw PacBio reads with homology to the single-copy region at the end of scaffold 14 (from 1 to 12 kb) were reassembled and analyzed for mutations not detected from the curated genome assembly. An example of an alternative assembly of the region detects a deletion in *smooth-19* not seen in the reference assembly. (C) All five *smooth* mutants exhibit a different polymorphism rate than the wild-type rate at a transition point between a high-copy-number transposon-containing region and a moderate-copy-number region of short, tandem repeats.

seven of these alternative contigs harbor mutations in at least one of the *smooth* strains (Fig. 2B and C), while the seventh is a complete assembly of the ribosomal DNA (rDNA) locus (18S, 5.8S, and 28S rRNA) (28) with adjacent 5'-TTAGTCAGGG-3' tandem repeats. These results suggest that all five *smooth* mutants harbor mutations in a related locus with short tandem repeats and rDNA repeats.

Repeat analysis of the FKP355 genome and *smooth* mutants. Given that the mutations identified in the *smooth* strains affected tandem repetitive DNA, we decided to more thoroughly assess the repetitive DNA content of the FKP355 genome. To avoid biases from the genome assembly process, we again examined the DNA directly in 150-bp Illumina sequencing reads from strain FKP355 for the presence of tandem repeats to identify and define all the telomere-like repetitive sequences present in this strain. All possible tandem duplications of unit size 1 to 75 bp were quantified in the raw sequencing reads, and the copy number of each repeat was estimated as follows:

$$\text{Copy number} = \frac{\text{Times found} \times \text{Genome size}}{\text{Total reads} \times (\text{Read length} - \text{Repeat length} + 1)}$$

The most overrepresented tandem repeat sequences identified in the FKP355 genome correspond to the 5'-TTAGTCAGGG-3' 10-mer found at the end of scaffold 14 as well as derivations on a 5'-TTGACGAGGCAC-3' 12-mer on its own and in combination with

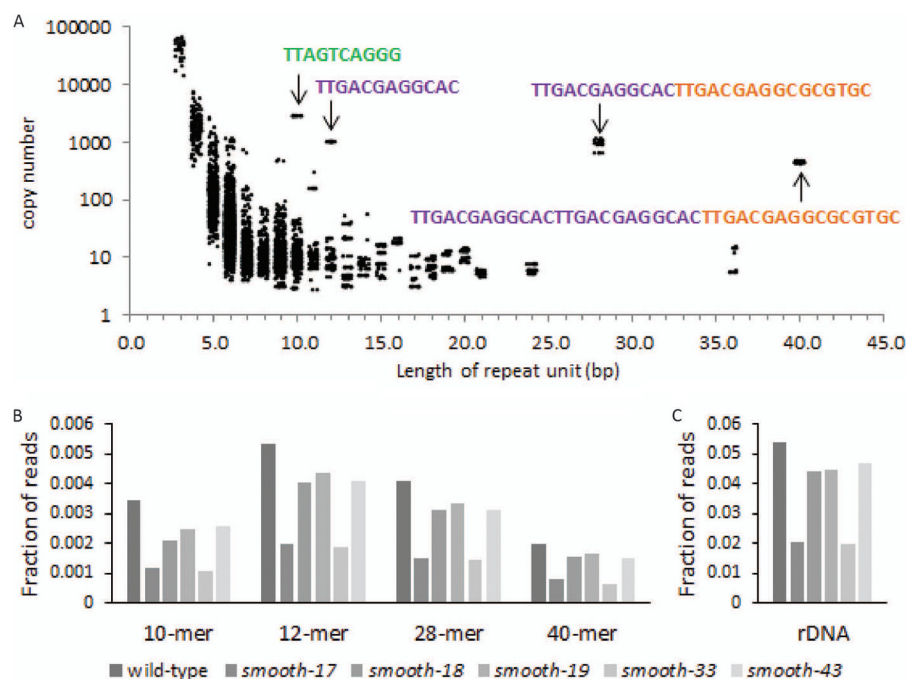


FIG 3 *smooth* strains have reduced repetitive DNA content. (A) Illumina 150-bp sequencing reads from strain FKP355 were systematically analyzed for the presence of all possible tandem duplications with a repeat unit length of 1 to 75 bp and quantified. Identification of phased repeat units with similar coverage was used to infer arrays of tandem repeats longer than a simple duplication. Colors indicate overlapping sequence motifs found in similar repeat sequences. (B) The fraction of 150-bp sequencing reads from the wild-type and *smooth* strains containing high-frequency tandem duplications of 10, 12, 28, and 40 bp in length. (C) The fraction of 150-bp sequencing reads from the wild-type and *smooth* strains that align to the FKP355 rDNA repeat.

a 5'-TTGACGAGGCGCGTGC-3' 16-mer (Fig. 3A). A number of low-copy-number polymorphic variations on these repeat sequences were also identified. Long PacBio sequencing reads from strain FKP355 containing tandem duplications of the 5'-TTAGTCAGGG-3' repeat unit were identified and aligned to the FKP355 genome assembly to identify additional repetitive and/or single-copy loci adjacent to this repeat array but found the end of scaffold 14 as the only nonrepetitive assembled portion of the genome adjacent to a 5'-TTAGTCAGGG-3' repeat array. This result suggests that either a single large 5'-TTAGTCAGGG-3' repeat array is present in the genome or that additional 5'-TTAGTCAGGG-3' repeat arrays are present but bordered by alternative unassembled repetitive DNA sequences consistent with subtelomere structural arrangements in yeast (29) and humans (30).

We identified individual long PacBio reads from strain FKP355 containing each of the short tandem 10- to 40-bp repeat elements as well as those mapping to the assembled rDNA locus to test how often different repeat sequences cooccurred. Roughly 11% of the long reads with a tandem 10-mer 5'-TTAGTCAGGG-3' repeat also mapped to the rDNA locus, while a higher percentage of the reads with a 5'-TTGACGAGGCAC-3' derived tandem repeat (49% of the 12-mer, 52% of the 28-mer, and 32% of the 40-mer) also mapped to the rDNA locus. Together, these results suggest that short tandem repetitive DNA is interspersed with the rDNA repeats.

We hypothesized that changes in the repetitive DNA content of the genome might underlie the *smooth* phenotype. Thus, the number of Illumina sequencing reads containing each of the different repeat units was assessed in the wild-type strain and each of the *smooth* mutants to quantify repetitive DNA content in a reference genome agnostic manner (Fig. 3B). All the *smooth* mutants have a decrease in short tandem repetitive DNA content with the greatest losses in the *smooth-17* and *smooth-33* mutants. These two mutants present a similar deletion when mapped to the FKP355

TABLE 1 Enriched Gene Ontology terms in the *smooth-33* mutant^a

GO term	FDR
Upregulated in the <i>smooth-33</i> mutant	
DNA repair	1.2E−05
Regulation of transcription from RNA polymerase II promoter	5.7E−04
DNA recombination	5.8E−03
DNA replication initiation	1.7E−02
Cell cycle process	3.3E−02
Mismatched DNA binding	3.3E−02
Nucleosome assembly	4.2E−02
Downregulated in the <i>smooth-33</i> mutant	
Small-GTPase-mediated signal transduction	1.8E−03
Steroid biosynthetic process	4.0E−03
GTP catabolic process	4.9E−03
Cytokinesis	1.7E−02
Nucleocytoplasmic transport	2.7E−02
Cellular lipid metabolic process	3.5E−02
Oxygen transport	3.6E−02
Membrane raft organization	3.6E−02
Chitin metabolic process	4.2E−02
Response to toxic substance	4.2E−02
Regulation of molecular function	4.5E−02
Fungal-type cell wall organization	4.5E−02
Microtubule-based movement	4.9E−02

^aAnalysis of the top 1,000 up- and downregulated genes identified biological process Gene Ontology (GO) terms specifically overrepresented in the *smooth-33* mutant (false-discovery rate [FDR] of <0.01).

reference genome (Fig. 2). The number of reads mapping to the rDNA locus was also assessed, as there appears to be at least some rDNA that is genetically linked to the end of scaffold 14 as well as the 10-mer 5'-TTAGTCAGGG-3' tandem repeats. All the *smooth* mutants have relatively fewer reads that map to the rDNA locus in a ratio similar to that of the short tandem repeat sequences (Fig. 3C). This suggests that the rDNA and the short tandem repeats together make up a repetitive part of the genome that is lost in the *smooth* mutants. We unsuccessfully attempted to reconstruct these complex mutations by transforming the wild-type parent (FKP355) with resistance marker constructs designed to randomly replace large tracts of repetitive DNA (data not shown). Thus, while the loss of repetitive DNA in the *smooth* mutants is intriguing, it has not been verified to be the cause of the *smooth* phenotype.

Transcriptome analysis of a *smooth* mutant. We compared gene expression from a prototrophic *smooth-33* mutant (FKP514) to a prototrophic wild-type strain of the same genetic background (FKP391) in chemostat culture to assess the effect on gene expression. Differentially expressed genes were analyzed for enrichment of Gene Ontology terms to assess specific biological processes perturbed in the *smooth-33* mutant (Table 1). Genes associated with DNA replication and repair as well as transcriptional regulation are more highly expressed in the *smooth-33* strain, while genes associated more generally with signaling, as well as membrane and cell wall biochemistry are downregulated. The promoter regions of differentially expressed genes were analyzed for enrichment of short DNA motifs to identify regulatory pathways acting through sequence-specific DNA-protein interactions. Genes upregulated in the *smooth-33* mutant are enriched for 5'-ACGCG-3' motifs in their promoters, while genes downregulated in the *smooth-33* mutant are enriched for 5'-CCCCT-3' motifs in their promoter region (E value < 0.05). We assessed the differential expression levels of genes with zero or more of these motifs near the transcription start site to confirm a specific effect on gene expression (Fig. 4). The presence of 5'-ACGCG-3' near the transcription start site has a slight positive effect on expression level in the *smooth-33* mutant. This is primarily associated with the presence of no less than two 5'-ACGCG-3' sites within 200 bp 5' and 1,000 bp 3' of the transcription start site. The presence of 5'-CCCCT-3' both 5' and 3' of the transcription start site is associated with a large

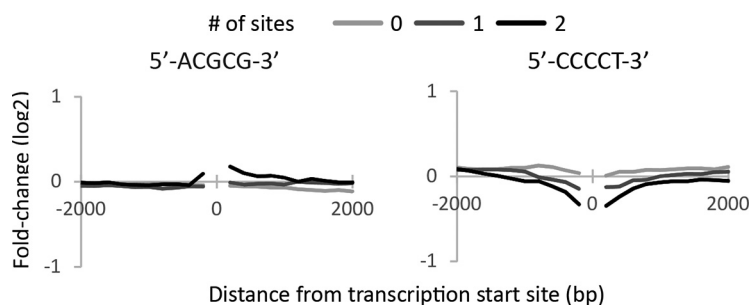


FIG 4 Effect of *smooth-33* on expression of genes with specific DNA motifs near their transcription start site. The number of ACGCG and CCCCT motifs on each strand of DNA was determined (from 0 to 2 sites) between the transcription start site (labeled 0) and a given distance. The given distances shown are 200 to 2,000 bp in 200-bp intervals, both up- and downstream of the transcription start site. For each interval, the average difference in expression between FKP514 (*smooth-33*) and FKP391 (wild type) during chemostat cultivation is shown. Note that the presence of more CCCCT motifs close to the transcription start site is generally associated with decreased expression in the *smooth-33* mutant, while the presence of more than one ACGCG site very near and 3' of the transcription start site is associated with increased expression in the *smooth-33* mutant.

negative effect on the expression level in the *smooth-33* mutant in a manner that increases with the number of 5'-CCCCT-3' sites.

We searched the Jaspar core fungal motifs database (31) for proteins that are known to interact with either of these motifs. A number of transcription factors from *S. cerevisiae* have been identified that interact specifically with the 5'-CCCCT-3' DNA motif via their C2H2 zinc finger domain(s). These transcription factors include Msn4p, Rgm1p, Rei1p, Rph1p, Msn2p, Gis1p, Com2p, and Usv1p (E value < 1). Comparison of these factors with proteins encoded by the *Y. lipolytica* genome (32) identified four C2H2 zinc finger domain-containing homologs (Table 2). The 5'-ACGCG-3' motif interacts with the cell cycle regulator proteins Mbp1p, Swi6p, and Swi4p in *S. cerevisiae* (E value < 1) via an APSES DNA interaction domain (33). Comparison of these proteins with proteins encoded by the *Y. lipolytica* genome (32) identified two homologs (Table 2). We attribute the presence of fewer genes to the whole-genome duplication event in *S. cerevisiae* which generated many paralogs represented by a single gene in *Y. lipolytica* (34).

Reverse genetics screen. We hypothesized that downregulation of genes with 5'-CCCCT-3' promoter motifs in the *smooth-33* strain is controlled by a C2H2 zinc finger transcription factor. Of the four transcription factors predicted to bind this motif in *Y. lipolytica*, one (JGI protein ID 143137; *Ylmsn2*) is very significantly downregulated (Table 2), which suggests that it may be an activator that is failing to regulate genes important for the yeast-to-hyphae transition in the *smooth-33* mutant. To test this, we overexpressed *Ylmsn2* using a constitutive promoter in a *smooth-33* strain and deleted it in the wild-type parent used for the mutagenesis screen. We found that overexpression of *Ylmsn2* restores hyphal growth in the *smooth-33* mutant, while deletion of

TABLE 2 Expression of *Y. lipolytica* genes predicted to regulate the *smooth* phenotype^a

JGI protein ID	<i>S. cerevisiae</i> homolog(s)	Log ₂ fold change	P value
5'-CCCCT-3' binding			
143137	<i>msn2</i> , <i>msn4</i> , <i>com2</i>	-2.63	3.46E-04
121652	<i>rei1</i>	0.90	4.68E-03
110816	<i>rph1</i> , <i>gis1</i>	0.61	4.76E-02
129649	<i>usv1</i> , <i>rgm1</i>	0.20	1.82E-01
5-ACGCG-3' binding			
13938	<i>swi6</i>	0.84	2.98E-03
129847	<i>swi4</i> , <i>mbp1</i>	0.84	6.32E-03

^aFold change and P values represent the change in expression level between the *smooth-33* and wild-type strains during chemostat cultivation.

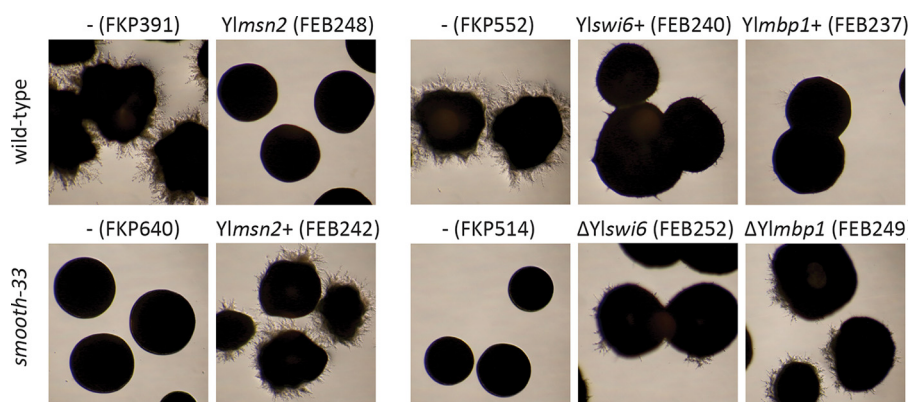


FIG 5 Ylmsn2p and the MBP complex regulate formation of hyphae. Ylmsn2p is predicted to interact with CCCCT promoter motifs, while the MBF complex (composed of Ylswi6p and Ylmbp1p) is predicted to interact with ACGCG motifs. Ylmsn2 was overexpressed in a *smooth-33* background and deleted in the parental hyphal background used for mutagenesis (FKP355). Conversely, Ylswi6 and Ylmbp1 were independently deleted in a *smooth-33* background and overexpressed in the parental background. Strains were cultured on YNB agar for 3 days at 28°C prior to examination of hyphae formation and imaging. Detailed genotypes are listed in Table 4.

Ylmsn2 results in loss of hyphal growth in wild-type *Y. lipolytica*, confirming its important role in regulation of this process and promotion of hyphal induction when expressed (Fig. 5).

We hypothesized that upregulation of genes with 5'-ACGCG-3' promoter motifs in the *smooth-33* strain is controlled by Ylswi6 (JGI protein ID 13938) and Ylmbp1 (JGI protein ID 129847), which form a complex that regulates the G₁/S phase transition in *S. cerevisiae* (35). Both of these genes are significantly upregulated in the *smooth-33* mutant (Table 2), suggesting promotion of the G₁/S transition during yeast phase growth. We hypothesized that lower expression of these important cell cycle regulators in wild-type strains is associated with the transition to hyphal growth. To test this, we overexpressed Ylswi6 or Ylmbp1 using a constitutive promoter in the wild-type parent strain and deleted them in the *smooth-33* strain. We found that deletion of Ylswi6 or Ylmbp1 restores some hyphal growth in the *smooth-33* mutant, while overexpression of Ylswi6 or Ylmbp1 results in reduced hyphal growth in wild-type *Y. lipolytica*, confirming that these genes play a role in regulation of the yeast-to-hyphae transition process (Fig. 5).

Isolation of mutants reverting to hyphal growth in the *smooth-33* background.

The success of our reverse genetic screen suggested that we may be able to identify additional factors regulating the yeast-to-hyphae transition via a forward genetic screen. Prototrophic *Y. lipolytica* *smooth-33* strain FKP514 was thus mutagenized with ethyl methanesulfonate (EMS) and plated on YNB agar plates to screen for colonies reverting to hyphal growth typical of wild-type *Y. lipolytica* on YNB. Approximately 500,000 colonies were screened, but no mutants were found that had reverted to a colony morphology typical of the wild type. However, 100 mutants were isolated that did not make completely smooth colonies. These mutants often appeared ruffled as colonies and upon microscopic observation appeared to have elongated cells and/or hyphae around their margins.

Identification of mutations promoting the yeast-to-hyphae transition in the *smooth-33* background. Twenty-eight of the hyphal mutants were sequenced using Illumina paired-end 150-bp sequencing and compared to the FKP355 reference genome to identify causative mutations. This initial search identified many genes with nonsynonymous mutations. Five genes were identified with nonsynonymous mutations in more than one mutant strain (JGI protein IDs 113409, 140296, 127631, 122144, and 109080), indicating that these genes are likely to be either the causative mutation or present at a hypermutable locus. The screen also identified four genes (JGI protein IDs 124736, 128138, 131882, and 129277) hit in only one mutant that are implicated in

TABLE 3 High-confidence genes involved in yeast-to-hyphae transition^a

JGI protein ID	<i>S. cerevisiae</i> BlastP ^b	No. of strains	Predicted mutations recovered
113409	<i>sln1</i> (<i>nik1</i>)	5	E342G, S441T, I536M, G584S, M598K
140296	<i>cts1</i>	4	K2*, W134*, G285E, G284V/E837D
127631	<i>ssk2</i>	3	G1190D, P555H, R526P
109080	<i>sln1</i> (<i>chk1</i>)	2	T1290M, E1415K
122144	<i>pbs2</i>	2	2 × G371R
124736	<i>hog1</i>	1	S335*
128138	<i>hym1</i>	1	L103P
131882	<i>lrg1</i>	1	G938C
129277	<i>mih1</i>	1	Y476*

^aGenes with mutations in independent mutant strains as well as genes found in only one strain but with few or no other nonsynonymous mutations. Eight mutant strains contained many nonsynonymous mutations in unique gene hits and are not shown.

^bGenes in parentheses represent the best BlastP hit from *C. albicans*.

the yeast-hyphal transition in other species and present in a mutant with a low background mutation rate, indicating that they are likely to be the causative mutation (summarized in Table 3). Eight of the mutant strains had many nonsynonymous mutations, making prediction of a likely causative mutation difficult.

Five of the high-confidence gene hits appear to be homologous to genes in the high-osmolarity glycerol response (HOG) MAPK signaling pathway of *S. cerevisiae*. We recovered three independent alleles of the MAPK kinase kinase YLssk2, two independent mutants with the same allele of the MAPK kinase Ylpbs2, and one mutant with a premature stop mutation in the MAPK Ylhog1 (Fig. 6 and Table 3). In addition, we identified mutations in two genes with similarity to the *sln1* histidine phosphotransfer kinase, which regulates the HOG MAPK cascade in *S. cerevisiae* (36, 37). Further investigation into the structure of the mutated genes within the context of the histidine kinase gene family in *Y. lipolytica* revealed that proteins 113409 and 109080 (JGI protein IDs) are not orthologous to the *sln1/ssk1* two-component regulator (38) known to regulate the HOG MAPK cascade in *S. cerevisiae*. Rather, they represent proteins not found in *S. cerevisiae* that are orthologous to the *nik1* and *chk1* genes of *C. albicans* respectively (39, 40) (Fig. 7A). In *C. albicans*, both the histidine kinases *nik1* and *chk1*, as well as the *sln1* ortholog are involved in hyphal formation (41). Disruption of any of these genes impairs hyphal formation, while double disruption of *sln1* or *nik1* in combination with *chk1* partially restores hyphal formation (41). We disrupted Ylchk1 in both the wild-type and *smooth-33* genetic background to assess its function in *Y. lipolytica* and to partially validate the results of the genetic screen. While Ylchk1 is not required for hyphal formation, deletion in the *smooth-33* background partially restores hyphal formation consistent with the results obtained for the Ylchk1 point mutants (Fig. 8).

The mutations isolated in Ylnik1 are nonrandomly distributed (Fig. 7B). In Ylnik1, all five mutations occur within a series of HAMP domain repeats (42). These repeats are associated with fungicide sensing (43–46) and mutation of the HAMP domain in bacterial receptor histidine kinases is associated with constitutive activation (47–49). The very specific site of the five mutations present in Ylnik1 from amino acids 342 to 598 (Table 3) and the lack of any putative nonfunctional mutations (e.g., premature stop codons or kinase functional domain mutations) suggests that Ylnik1p may be constitutively activated in these mutants and that the hyphal phenotype is caused by constitutive signaling rather than loss of function.

Three genes were recovered in single mutant strains known to be involved in morphogenesis in *S. cerevisiae*, including *hym1* (50), the GTPase-activating protein *lrg1* (51), and the tyrosine phosphatase *mih1* (52). Four independent mutations were found in the endochitinase *cts1* in strains with weaker colony morphology phenotypes typical of hyphal growth. Close observation revealed the morphology phenotype was due to a cell separation defect, as has been found in *S. cerevisiae* (53), rather than a switch to hyphal growth. These mutants were not considered further in this work.

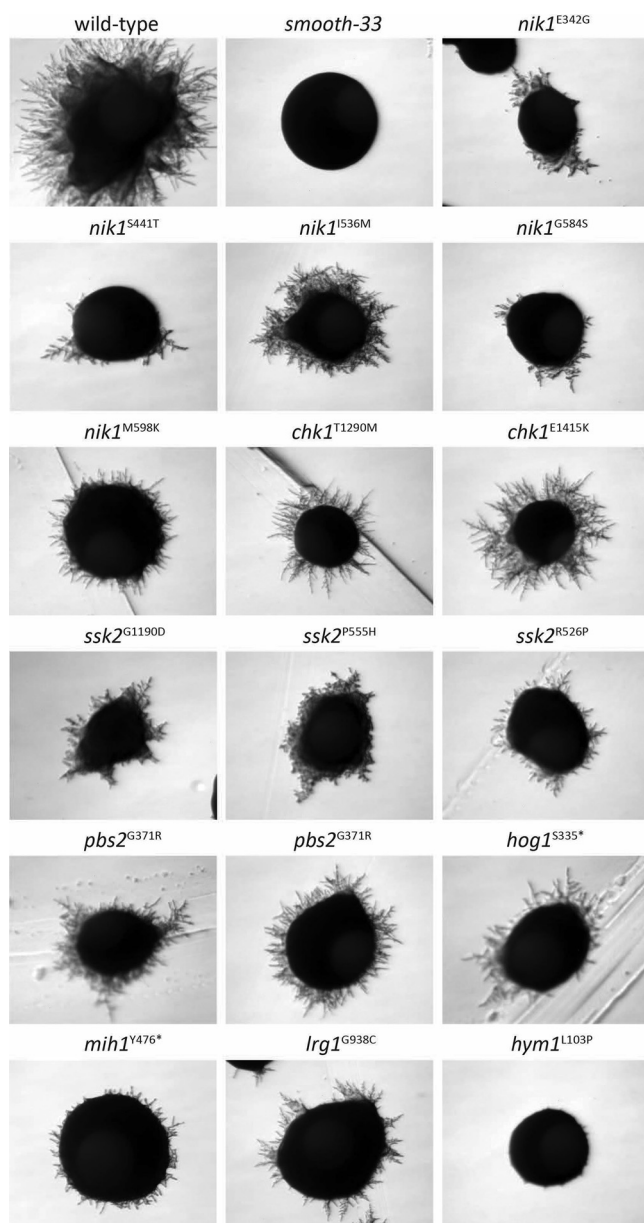


FIG 6 Mutants with a hyphal reversion phenotype in *smooth-33*. FKP514 (*smooth-33*) was mutagenized, and colonies exhibiting a transition to hyphal growth were isolated and sequenced. Mutant strains were plated on YNB agar, and isolated single colonies were imaged after 48 h at 28°C. Gene names shown are based on orthologs from *S. cerevisiae* and *C. albicans*. Mutations shown are the highest likelihood candidate identified after sequencing of each mutant.

DISCUSSION

Development of yeast strains that do not switch between yeast and hyphal growth is critical for the utilization of fungi in reproducible bioprocesses. In this work, we isolated five spontaneous *Y. lipolytica* mutants that grow only in the yeast phase and do not form hyphae when cultivated on solid agar or in liquid medium in flasks or during bioreactor cultivation (Fig. 1). These mutants, which we named *smooth* mutants, were screened for rapid growth and nonreversion of the phenotype to identify strains useful for genetic engineering efforts toward the production of biofuels and chemicals with a *Y. lipolytica* host chassis. Genomic analysis of the *smooth* mutants revealed that all share mutation of a repetitive locus resulting in loss of short repetitive telomere-like DNA and rDNA repeats (Fig. 2 and 3). Transcriptome analysis of a selected mutant

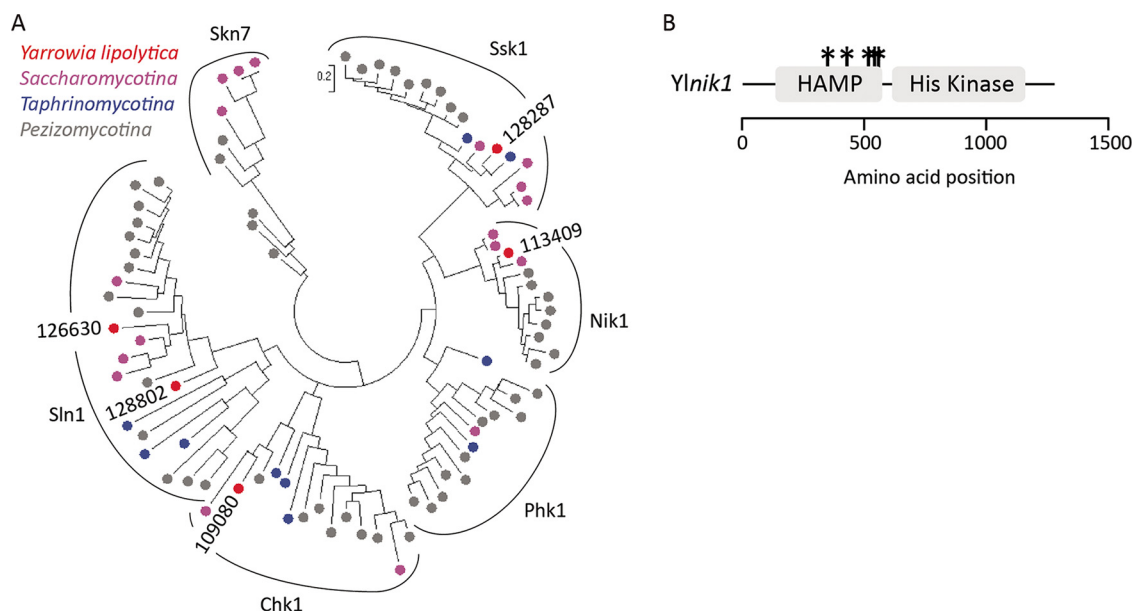


FIG 7 Histidine kinases in *Y. lipolytica*. (A) Phylogenetic reconstruction of selected histidine kinases from ascomycete fungi. Protein sequences from the histidine kinases of *Y. lipolytica* with similarity to Sln1p (FKP355 JGI protein ID 128287, 113409, 109080, 128802, and 126630) were used as bait to BlastP search the proteomes of *Y. lipolytica*, *S. cerevisiae*, *C. albicans*, *Lipomyces starkeyi*, *Schizosaccharomyces pombe*, *Taphrina deformans*, *Ascobolus immerses*, *Monascus purpureus*, *Aspergillus nidulans*, *Stagnospora nodorum*, *Cladonia grayi*, *Botrytis cinerea*, *Neurospora crassa*, and *Xylaria heveae*. The BlastP hits were aligned using MUSCLE and analyzed by the maximum likelihood method with 200 bootstrap replicates to define the relationships between the *Y. lipolytica* genes and those from other species. (B) Protein domains from Ylnik1p were predicted by InterProScan (90). The kinase domain in Ylnik1p is predicted to be an S/T protein kinase. Note that all the mutations recovered occur in the HAMP domain. The sites of mutations are indicated by asterisks.

(*smooth-33*) revealed specific DNA motifs in the promoter regions of up- and down-regulated genes (Fig. 4). These short DNA motifs implicated specific regulatory proteins important for maintenance of the yeast form which we confirmed by deletion and overexpression analysis (Fig. 5).

Our analysis identified the homolog of the stress response regulator *Ylmsn2* as a primary regulator of the yeast-to-hyphae transition in *smooth* mutants. This gene, previously identified as *mhy1* in *Y. lipolytica* (23) is essential for the yeast-to-hyphae transition (Fig. 5) and activates gene expression in response to general stresses by binding to the stress response element 5'-CCCCT-3' (23, 54). Loss of signaling through *Ylmsn2* in the *smooth* strains and frequent hyphal growth in the wild-type strain suggests that our typical laboratory growth conditions (YNB medium at 28°C) are stressful to *Y. lipolytica*. We observe more frequent initiation of hyphal growth on medium with a higher C/N ratio and less hyphae with a rich nitrogen source like peptone, which implicates nitrogen quantity and quality in this response (55). *Msn2p* is

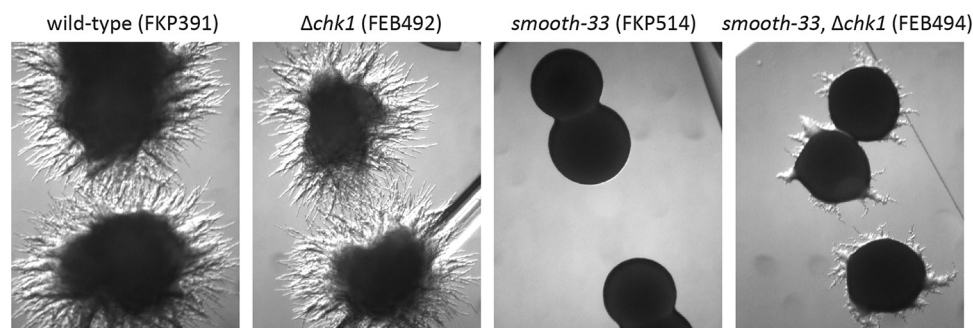


FIG 8 *Ylchk1* regulates formation of hyphae. *Ylchk1* was deleted in wild-type and *smooth-33* genetic backgrounds by replacement with *leu2*. *Ylchk1* is not required for the transition to hyphal growth morphology, but deletion results in limited reversion to hyphal morphology in *smooth-33*.

regulated by the TORC1-Sch9-Rim15 signaling pathway in *Y. lipolytica* (22), suggesting nutrient availability may be the inducer of hyphal growth in these experiments.

All five *smooth* strains exhibit what appear to be similar mutations in a poorly assembled, repetitive region of the genome represented by the end of scaffold 14 in the parent strain genome assembly (<http://genome.jgi.doe.gov/Yarlip1/Yarlip1.home.html>) (Fig. 2). Scaffold 14 ends in tandem 5'-TTAGTCAGGG-3' repeats characteristic of *Y. lipolytica* telomeres (26); however, the mutation in some of the *smooth* strains, particularly the *smooth-43* strain, extends into the unique portion of scaffold 14 and initially alerted us to examine the repetitive DNA content of the wild-type and *smooth* strains. An unbiased search for short tandem repeats confirmed that the 5'-TTAGTCAGGG-3' repeats are common and identified additional repetitive tandem DNA sequences present in the *Y. lipolytica* genome that are likely to constitute the telomere and subtelomere regions. Analysis of long PacBio reads found that many of these short repeats are bordered by rDNA repeats (28), and all repeat types are lost in similar quantity within each of the five *smooth* mutants (Fig. 3). Copy number variation in the rDNA repeats has been reported in filamentous fungi and yeasts and affects general physiological parameters, such as growth rate (56–59) and in *C. albicans* is associated with morphological mutants (60).

The complete mechanism governing loss of filamentous growth in the *smooth* mutants remains unclear. Our results indicate that expression changes in the *smooth* strains are governed primarily by reduced activation of genes with stress response elements by the transcription factor Msn2p (54, 61). Activation of the general stress response via Msn2p occurs through phosphorylation of the transcription factor by PKA and nuclear localization (62–64) and is dependent on cAMP signaling in response to a variety of nutritional and environmental stresses (65). We found that cell cycle progression genes are upregulated in the *smooth-33* mutant and that disruption of either component of the G₁/S transition-promoting MBF complex (Mbp1p/Swi6p) (66, 67) conferred a sporadic low-level return to filamentous growth (Fig. 5). Together, these results suggest that the loss of repetitive telomeric and ribosomal DNA repeats is reducing signaling via the general stress response and promoting cell cycle progression.

We performed a forward genetic screen for reversion to hyphal growth in a prototrophic *smooth-33* strain to better understand the signaling occurring in response to the loss of repetitive telomeric and ribosomal DNA at the *smooth* locus (selected mutant phenotypes in Fig. 6). From this screen, 28 mutants were sequenced by high-throughput sequencing, and interestingly, we did not identify strains with mutations in *Ylmbp1* or *Ylswi6*. This suggests that the screen was not exhaustive for recovery of mutants with a sporadic reversion phenotype, as we sequenced the subset with the strongest hyphal phenotype maintained in all colonies after passaging and replating. Examination of the mutations in these strains implicates the histidine kinases *Ylnik1* and *Ylchk1* as well as the core components of the HOG MAPK cascade (*Ylssk2*, *Ylpbs2*, and *Ylhog1*) in regulation of the yeast-to-hyphae transition in *Y. lipolytica*. In *C. albicans*, *nik1* and *chk1* are required for normal hyphal growth (41). Here we found that *Ylchk1* is not required for hyphal growth (Fig. 8). The mutations recovered in *Ylnik1* all occur only in the sensory HAMP domain (Fig. 7). Deletion of the HAMP domain in *C. albicans nik1* strain results in constitutive signaling as well as phosphorylation and activation of Hog1p (68). No mutations predicted to be nonfunctional were recovered in *Ylnik1*, suggesting that reversion to hyphal growth is due to constitutive or altered activation of this kinase.

Nik1p and Chk1p represent the common type III and type X histidine kinases that govern morphogenesis and enable pathogenicity in many fungi (69). Localization studies in *Candida guilliermondii* found that unlike the membrane-localized type VI histidine kinase, Sln1p, Nik1p, and Chk1p both localize to the cytosol and nucleus (70). While both Nik1p and Chk1p have been demonstrated to respond to general stresses by signaling to downstream targets, their method of sensing stresses has not been determined. Genetic studies have found that the nonkinase domains are required for sensing stresses, but further work is needed to determine how extracellular stresses alter the structure and activity of these cytoplasmic proteins (70). These histidine

TABLE 4 *Y. lipolytica* strains used in this study

Strain	Genotype	Reference
FKP355	<i>matA leu2-270 xpr2-332 axp-2 ku70::hph⁺</i>	55
FKP391	<i>matA leu2-270::leu2⁺ xpr2-332 axp-2 ku70::hph⁺</i>	55
FKP500	<i>matA leu2-270 xpr2-332 axp-2 ku70::hph⁺ smooth-17</i>	This work
FKP501	<i>matA leu2-270 xpr2-332 axp-2 ku70::hph⁺ smooth-18</i>	This work
FKP502	<i>matA leu2-270 xpr2-332 axp-2 ku70::hph⁺ smooth-19</i>	This work
FKP503	<i>matA leu2-270 xpr2-332 axp-2 ku70::hph⁺ smooth-33</i>	This work
FKP504	<i>matA leu2-270 xpr2-332 axp-2 ku70::hph⁺ smooth-43</i>	This work
FKP514	<i>matA leu2-270::leu2⁺ xpr2-332 axp-2 ku70::hph⁺ smooth-33</i>	This work
FEB248	<i>matA leu2-270 xpr2-332 axp-2 ku70::hph⁺ msn2::leu2⁺</i>	This work
FKP552	<i>matA leu2-270 xpr2-332 axp-2 ku70::hph⁺ exp1p::leu2⁺</i>	This work
FEB237	<i>matA leu2-270 xpr2-332 axp-2 ku70::hph⁺ exp1p-mbp1::leu2⁺</i>	This work
FEB240	<i>matA leu2-270 xpr2-332 axp-2 ku70::hph⁺ exp1p-swi6::leu2⁺</i>	This work
FKP640	<i>matA leu2-270 xpr2-332 axp-2 ku70::hph⁺ smooth-33 exp1p::leu2⁺</i>	This work
FEB242	<i>matA leu2-270 xpr2-332 axp-2 ku70::hph⁺ smooth-33 exp1p-msn2::leu2⁺</i>	This work
FEB249	<i>matA leu2-270 xpr2-332 axp-2 ku70::hph⁺ smooth-33 mbp1::leu2⁺</i>	This work
FEB252	<i>matA leu2-270 xpr2-332 axp-2 ku70::hph⁺ smooth-33 swi6::leu2⁺</i>	This work
FKP672	<i>matA leu2-270::leu2⁺ xpr2-332 axp-2 ku70::hph⁺ smooth-33 mih1^{Y476*}</i>	This work
FKP673	<i>matA leu2-270::leu2⁺ xpr2-332 axp-2 ku70::hph⁺ smooth-33 lrg1^{G938C}</i>	This work
FKP675	<i>matA leu2-270::leu2⁺ xpr2-332 axp-2 ku70::hph⁺ smooth-33 nik1^{E342G}</i>	This work
FKP677	<i>matA leu2-270::leu2⁺ xpr2-332 axp-2 ku70::hph⁺ smooth-33 nik1^{S441T}</i>	This work
FKP681	<i>matA leu2-270::leu2⁺ xpr2-332 axp-2 ku70::hph⁺ smooth-33 nik1^{S36M}</i>	This work
FKP682	<i>matA leu2-270::leu2⁺ xpr2-332 axp-2 ku70::hph⁺ smooth-33 nik1^{G584S}</i>	This work
FKP683	<i>matA leu2-270::leu2⁺ xpr2-332 axp-2 ku70::hph⁺ smooth-33 nik1^{M598K}</i>	This work
FKP684	<i>matA leu2-270::leu2⁺ xpr2-332 axp-2 ku70::hph⁺ smooth-33 pbs2^{G371R}</i>	This work
FKP686	<i>matA leu2-270::leu2⁺ xpr2-332 axp-2 ku70::hph⁺ smooth-33 ssk2^{G1190D}</i>	This work
FKP687	<i>matA leu2-270::leu2⁺ xpr2-332 axp-2 ku70::hph⁺ smooth-33 hog1^{R335*}</i>	This work
FKP689	<i>matA leu2-270::leu2⁺ xpr2-332 axp-2 ku70::hph⁺ smooth-33 chk1^{T1290M}</i>	This work
FKP690	<i>matA leu2-270::leu2⁺ xpr2-332 axp-2 ku70::hph⁺ smooth-33 ssk2^{P555H}</i>	This work
FKP691	<i>matA leu2-270::leu2⁺ xpr2-332 axp-2 ku70::hph⁺ smooth-33 ssk2^{R526P}</i>	This work
FKP694	<i>matA leu2-270::leu2⁺ xpr2-332 axp-2 ku70::hph⁺ smooth-33 chk1^{E1415K}</i>	This work
FKP695	<i>matA leu2-270::leu2⁺ xpr2-332 axp-2 ku70::hph⁺ smooth-33 pbs2^{G371R}</i>	This work
FKP730	<i>matA leu2-270::leu2⁺ xpr2-332 axp-2 ku70::hph⁺ smooth-33 hym1^{L103P}</i>	This work
FEB492	<i>matA leu2-270 xpr2-332 axp-2 ku70::hph⁺ chk1::leu2⁺</i>	This work
FEB494	<i>matA leu2-270 xpr2-332 axp-2 ku70::hph⁺ smooth-33 chk1::leu2⁺</i>	This work

kinases, particularly *nik1*, are implicated in activation of the HOG pathway. However, it remains to be determined whether this affect is direct (e.g., through phosphorylation of HOG MAPK components) or a result of stress caused by their constitutive signaling.

In summary, we examined *Y. lipolytica* mutants that do not transition to hyphal morphology under conditions relevant to industrial production of biofuels and commodity chemicals. We identified mutations in the repetitive DNA of these strains that reduce signaling through the general stress response pathway via an unknown mechanism. Reversion to hyphal growth is possible in these mutants via signaling or lack thereof by *Ylmsn2*, the HOG MAPK cascade components (*Ylssk2*, *Ylpbs2*, and *Ylhog1*), and the histidine kinases encoded by *Ylnik1* and *Ylchk1*. This work builds upon our understanding of the dimorphic transition in *Y. lipolytica* and confirms that the pathways regulating this morphological switch are conserved with other ascomycete yeasts. How the loss of repetitive DNA reduces the *msn2*-mediated stress response remains an enigma. Eleven of the mutants recovered in the reversion to hyphal growth screen warrant further analysis and may shed light on the connection between the loss of repetitive DNA and reduction of the stress response.

MATERIALS AND METHODS

Yeast cultivation and forward genetic screens for nonhyphal mutants. All *Y. lipolytica* strains used in this study (Table 4) were maintained in YNB (1.7 g/liter yeast nitrogen base without amino acids and ammonium sulfate but with 20 g/liter glucose and 5 g/liter ammonium sulfate) or YPD (10 g/liter peptone, 10 g/liter yeast extract, 20 g/liter glucose) liquid medium at 28°C and 200 rpm unless otherwise noted. Auxotrophs were supplemented with 0.1 g/liter leucine when appropriate. Frozen stocks were maintained at −80°C in 15% glycerol. To isolate *smooth* mutants, *Y. lipolytica* strain FKP355 was passaged daily in YPD for 2 weeks to allow accumulation of mutations and plated at a density of 10,000 cells per plate on YNB agar plates. Plates were incubated 72 h at 28°C to allow development of colonies. Large

colonies without hyphae were streaked onto fresh YNB plates to obtain pure mutant strains. Purified mutant strains were inoculated onto YPD, YNB, and YNB150 (1.7 g/liter yeast nitrogen base without amino acids and ammonium sulfate but with 25 g/liter glucose and 0.367 g/liter ammonium sulfate) agar plates to confirm the phenotype. To isolate *smooth* mutants reverting to hyphal growth, *Y. lipolytica* strain FKP514 was mutagenized with ethyl methanesulfonate (EMS) (71) and plated at a density of 10,000 cells per plate on YNB agar plates. Plates were incubated 72 h at 28°C to allow development of colonies. Colonies exhibiting ruffled morphologies characteristic of the transition to hyphal growth were streaked onto fresh YNB plates to obtain pure mutant strains. Chemostat cultivation was performed with a dilution rate of 0.05 per hour at 30°C in a 1.2-liter bioreactor (DASGIP, Jülich, Germany) with a working volume of 750 ml at pH 3.5, controlled with 2 M KOH. Dissolved oxygen was kept above 30% with a stirrer rate of 600 rpm and an airflow rate of 1 v.v.m. The growth medium contained 25 g/liter glucose, 0.5 g/liter (NH₄)₂SO₄, 5.96 g/liter K₂SO₄, 3 g/liter KH₂PO₄, 0.5 g/liter MgSO₄·7H₂O, vitamins and trace metal solutions (72) and 125 µl antifoam 204 (Sigma-Aldrich, St. Louis, MO, USA). Samples for transcriptomic analysis were taken when the chemostats reached steady state, defined as stable CO₂ and O₂ outflow and optical density, which was achieved after circa 120 h.

Reference genome sequencing and assembly. Genomic DNA and RNA were isolated from *Y. lipolytica* strain FKP355 (55) using a yeast genomic DNA purification kit (AMRESCO, Solon, OH) and TRIzol reagent (Invitrogen, Carlsbad, CA), respectively. One microgram of DNA was sheared to 10 kb using the g-TUBE (Covaris). The sheared DNA was treated with DNA damage repair mix followed by end repair and ligation of SMRT adapters using the PacBio SMRTbell Template Prep kit (PacBio). The SMRTbell templates were then purified using exonuclease treatments and size selected using AMPure PB beads. Sequencing primer was then annealed to the SMRTbell templates, and Version P6 sequencing polymerase was bound to them. The prepared SMRTbell template libraries were then sequenced on a Pacific Biosciences RSII sequencer using Version C4 chemistry and 4-h sequencing movie run times. Filtered subread data were assembled together with Falcon version 0.4.2 (<https://github.com/PacificBiosciences/FALCON>) to generate an initial assembly. Mitochondria were then assembled separately using the corrected preads with Celera version 8.3 and subsequently polished with Quiver. It was then used to remove mitochondrial data from the preads. A secondary Falcon assembly was generated using the filtered preads with Falcon version 0.4.2 and polished with Quiver version smrtanalysis_2.3.0.140936.p5 (<https://github.com/PacificBiosciences/GenomicConsensus>). The final genome assembly was annotated using the JGI Annotation Pipeline (73).

Stranded cDNA libraries were generated using the Illumina Truseq Stranded RNA LT kit. mRNA was purified from 1 µg of total RNA using magnetic beads containing poly(T) oligonucleotides. mRNA was fragmented and reverse transcribed using random hexamers and SSII (Invitrogen) followed by second strand synthesis. The fragmented cDNA was treated with end pair, A-tailing, adapter ligation, and eight cycles of PCR. The prepared Illumina libraries were quantified using KAPA Biosystem's next-generation sequencing library qPCR kit and run on a Roche LightCycler 480 real-time PCR instrument. The quantified libraries were then multiplexed with other libraries, and the pool of libraries was then prepared for sequencing on the Illumina HiSeq 2500 sequencing platform utilizing a TruSeq paired-end cluster kit, v4, and Illumina's cBot instrument to generate a clustered flow cell for sequencing. Sequencing of the flow cell was performed on the Illumina HiSeq2500 sequencer using a TruSeq SBS sequencing kit, v4, following a 2 × 100 indexed run recipe.

Transcriptome raw fastq file reads were evaluated for artifact sequence using BBDuk (<https://sourceforge.net/projects/bbmap/>), raw reads by kmer matching (kmer = 25), allowing 1 mismatch and detected artifact was trimmed from the 3' ends of the reads. RNA spike-in reads, PhiX reads, and reads containing any Ns were removed. Quality trimming was performed using the phred trimming method set at Q6. Finally, following trimming, reads under the length threshold were removed (minimum length 25 bases or 1/3 of the original read length, whichever is longer). Filtered fastq files were used as input for *de novo* assembly of RNA contigs. Reads were assembled into consensus sequences using Trinity (ver. 2.1.1) (74) with the `-normalize_reads` (In-silico normalization routine) and `-jaccard_clip` (Minimizing fusion transcripts derived from gene dense genomes) options. The assembled transcriptome was used for genome annotation and made available through the JGI fungal genome portal MycoCosm (<http://genome.jgi.doe.gov/Yarlip1/Yarlip1.home.html>).

Genome resequencing and identification of mutations. Genomic DNA was prepared from wild-type and mutant strains using a yeast genomic DNA purification kit (AMRESCO, Solon, OH) followed by 150-bp paired-end sequencing on an Illumina MiSeq instrument or 100-bp paired-end sequencing on an Illumina HiSeq instrument (San Diego, CA). The paired-end reads were aligned to the *Y. lipolytica* FKP355 reference genome sequence available at the website <http://genome.jgi.doe.gov/Yarlip1/Yarlip1.home.html> using BWA (75) or Bowtie2 (76) and visualized with the Integrated Genomics Viewer (77). Mutations were identified and annotated with Samtools (78), Pindel (79), BreakDancer (80), CNVnator (81), SnpEff (82), and custom Perl scripts.

Overexpression plasmid construction. Overexpression plasmids were constructed using pYL15 as a vector (55). Coding sequences from *Ylmsn2*, *Ylmbp1*, and *Ylswi6* were PCR amplified using primer pairs OEB491/492, OEB497/498, and OEB503/504, respectively, from *Y. lipolytica* FKP355 genomic DNA using Q5 DNA polymerase (New England Biolabs, Ipswich, MA) (Table 5). Plasmid pYL15 was digested with SmaI and Fast AP (Fermentas, Waltham, MA) to dephosphorylate plasmid ends. The PCR products were purified using a GeneJET purification kit (Thermo Fisher Scientific, Waltham, MA) and assembled using the NEBuilder HiFi assembly kit (New England Biolabs, Ipswich, MA) according to the manufacturer's instructions to produce autonomously replicating overexpression plasmids for *msn2*, *mbp1*, and *swi6*.

TABLE 5 Primers used in this study

Primer	Sequence (5→3')
OKP443	ACCCGTTGCTATCTCCACAC
OKP444	GTGCAGTCGCCAGCTTAAA
OEB491	ATATCTACAGCGGTACCCCCATGGACCTCGAATTGGAAAT
OEB492	CCGCCTCCGCCGATATCCCCCTAGTCCCAGGATGCGTA
OEB497	ATATCTACAGCGGTACCCCCATGTCCATCTACAAAGCAAC
OEB498	CCGCCTCCGCCGATATCCCCCTATCTCTCCCTCAAGCA
OEB503	ATATCTACAGCGGTACCCCCATGCCGACGTGAAACACGA
OEB504	CCGCCTCCGCCGATATCCCCCTATGCTGCTGAGGAGGCT
OEB544	CTGATCGTACCTTGATGTCGACCCGTTGCTATCTCCACAC
OEB545	CGTACAGTTCGAGGATCGTAGTGCAGTCGCCAGCTTTAAA
OEB487	GGTTTTGAGTCTTGGGAGTGG
OEB548	CGACATCAAGGTACGATCAGATGGGCCAAAGTTAGTGGTG
OEB549	TACGATCCTCGAAGTGTACGCTTCTAGTCTCCGCTCCAT
OEB490	CCACAGCTGCTCTTATGACG
OEB493	GTAGTTTCGGTTGCCTCGTC
OEB550	CGACATCAAGGTACGATCAGTCGAGTTACCCTATGTGCTG
OEB551	TACGATCCTCGAAGTGTACGGGGTCGGTCTAGGACGATGT
OEB496	GACACAAAGCTCATCGGTGG
OEB499	TGCAATCTCTCCAGATT
OEB552	CGACATCAAGGTACGATCAGTGTCTGAACGCTTTGAGC
OEB553	TACGATCCTCGAAGTGTACGCTCACGGTATGGGCTGTTCT
OEB502	TCTCCGAGGCCATCATTAG
OEB846	TTGATCCTGATGGTCGTGAA
OEB847	CGACATCAAGGTACGATCAGATCAGCGGAGATGTTTCGTC
OEB848	TACGATCCTCGAAGTGTACGGAATAAACCGTCAGCCAGCA
OEB849	GGCGACACAGTCAGAGCATA
OEB4	CGGAGATGATATCGCCAAAC
OEB575	GAGCTGCCATTGAGAAGGAG

Yeast strain construction. Transformations were performed by the lithium acetate method (83), and transformants were selected on YNB agar. PCR products were amplified using Q5 DNA polymerase (New England Biolabs, Ipswich, MA) and custom primers (Table 5). DNA fragments were purified using a GeneJET purification kit (Thermo Fisher Scientific, Waltham, MA). *leu2-270* was complemented in FKP503 (*smooth-33*) by transformation with full-length *leu2* after PCR amplification using primer pair OKP443/444 to construct strain FKP514. Integration at the *leu2-270* locus was confirmed by PCR. *Ylmsn2*, *Ylmbp1*, *Ylswi6*, and *Ylchk1* were replaced with a *leu2⁺* nutritional marker. Briefly, 1-kb regions flanking each gene were amplified from FKP355 genomic DNA using Q5 DNA polymerase and primers designed with overhangs homologous to the *leu2* gene (amplified with primers OEB544/545) from *Y. lipolytica* genomic DNA (primer pairs OEB487/548, OEB549/490, OEB493/550, OEB551/496, OEB499/552, OEB553/502, OEB846/847, and OEB848/849). The fragments were purified using a GeneJET purification kit (Thermo Fisher Scientific, Waltham, MA) and assembled into full-length deletion cassettes with *leu2* using NEBuilder HiFi assembly kit or as split marker deletion cassettes with internal *leu2* primers OEB4 and OEB575. Deletion cassettes were transformed into strain FKP355 or FKP503 as appropriate. Replacement of genes with *leu2⁺* was confirmed by PCR. Deletion and overexpression strains were characterized on YNB agar at 28°C.

Transcriptome analysis. Samples for transcriptome analysis were collected from steady-state chemostats, frozen in liquid nitrogen, and stored at -80°C . Total RNA was extracted with TRIzol (Invitrogen, Carlsbad, CA, USA) following the manufacturer's instructions with additional mechanical disruption of the cells using a FastPrep homogenizer (MP Biomedicals, Santa Ana, CA, USA) and 1-mm silica beads. Further RNA preparation and RNA sequencing were performed by SciLifeLab in Uppsala, Sweden, using their IonTorrent platform. Raw RNA-seq reads were aligned to the *Y. lipolytica* genome using Bowtie (76), and counts were obtained with HTSeq (84) and transformed using voom (85). The top 1,000 genes with the greatest positive and negative fold change values from the FKP514 versus FKP391 transcriptome comparison were analyzed for enrichment of Gene Ontology terms using FunRich (86). The 500-bp promoter region of the top 1,000 genes with the greatest positive and negative fold change values from the FKP514 versus FKP391 transcriptome comparison were analyzed for enrichment of specific sequence motifs using DREME (87). Identified motifs were compared to the Jaspas core fungal motifs database (31) using Tomtom (88) to identify candidate regulators.

Microscopy. For confocal microscopy, live cells were collected and immediately visualized using a Zeiss LSM710 confocal laser-scanning microscope (Carl Zeiss Microimaging GmbH, Munchen, Germany) with a Plan-Apochromate 100 \times /1.4 oil objective. All images were processed using ImageJ (89). For colony morphology, cells were imaged on a VWR Stereo Zoom Trinocular microscope fitted with a Canon EOS 6D DSLR camera, and images were processed with Adobe Photoshop.

Data availability. Sequence data from the whole-genome shotgun project for *Y. lipolytica* FKP355 have been deposited at DDBJ/ENA/GenBank under accession number [PKSB000000000](#). The version of sequence data described in this paper has accession number [PKSB010000000](#). Sequence data for the *Y. lipolytica smooth* strains (FKP355 and FKP500 to FKP504) have been deposited at NCBI SRA under

accession number [PRJNA499126](#). Sequence data for the *Y. lipolytica* hyphal reversion strains (FKP514 to FKP730) have been deposited at NCBI SRA under accession numbers [SRP145806](#), [SRP145808](#), [SRP145807](#), [SRP145813](#), [SRP145810](#), [SRP145811](#), [SRP145814](#), [SRP145809](#), [SRP145815](#), [SRP145817](#), [SRP145820](#), [SRP145818](#), [SRP145816](#), [SRP145821](#), [SRP145825](#), [SRP145822](#), [SRP145824](#), [SRP145826](#), [SRP145835](#), [SRP145830](#), [SRP145834](#), [SRP145828](#), [SRP145836](#), [SRP145832](#), [SRP145831](#), [SRP145829](#), [SRP145833](#), [SRP145837](#), and [SRP145838](#). Transcriptome data have been deposited at ArrayExpress under accession number [E-MTAB-7400](#).

ACKNOWLEDGMENTS

This material is based upon work supported by the U.S. Department of Energy (DOE), Office of Science, Office of Biological and Environmental Research (OBER), Genomic Science program, under award DE-SC0008744. Support was also provided by a William Wiley postdoctoral fellowship to K.R.P., and by Åforsk foundation to E.J.K. The work conducted by the U.S. Department of Energy Joint Genome Institute, a DOE Office of Science User Facility, is supported by the Office of Science of the U.S. Department of Energy under contract DE-AC02-05CH11231. Work conducted by the DOE Joint BioEnergy Institute (<http://www.jbei.org>) was supported by the U.S. Department of Energy, Office of Science, Office of Biological and Environmental Research, through contract DE-AC02-05CH11231 between Lawrence Berkeley National Laboratory and the U.S. Department of Energy. Part of this research was performed at the Environmental Molecular Sciences Laboratory (EMSL), a national scientific user facility sponsored by the U.S. DOE OBER, and located at the Pacific Northwest National Laboratory (PNNL). Part of this research was supported by the Synthetic Biology – Agile within the LDRD Program at PNNL. PNNL is a multiprogram national laboratory operated by Battelle for the DOE under contract DE-AC05-76RLO 1830. Work conducted at Chalmers University of Technology was partly funded by the Novo Nordisk Foundation and the Knut and Alice Wallenberg Foundation.

We declare that we have no competing interests.

K.R.P., E.L.B., E.J.K., J.N., and S.E.B. conceived and designed the experiments. K.R.P., E.L.B., E.J.K., S.H., H.H., K.L., A.L., and M.Y. performed the experiments. K.R.P., E.L.B., E.J.K., and S.E.B. analyzed the data. K.R.P., E.J.K., E.L.B., K.B., J.K.M., I.V.G., B.A.S., and S.E.B. initiated and managed the genome sequencing, assembly, and analysis. All authors read and approved the final manuscript.

REFERENCES

- Bastidas RJ, Heitman J. 2009. Trimorphic stepping stones pave the way to fungal virulence. *Proc Natl Acad Sci U S A* 106:351–352. <https://doi.org/10.1073/pnas.0811994106>.
- Boyce KJ, Andrianopoulos A. 2015. Fungal dimorphism: the switch from hyphae to yeast is a specialized morphogenetic adaptation allowing colonization of a host. *FEMS Microbiol Rev* 39:797–811. <https://doi.org/10.1093/femsre/fuv035>.
- Huang G. 2012. Regulation of phenotypic transitions in the fungal pathogen *Candida albicans*. *Virulence* 3:251–261. <https://doi.org/10.4161/viru.20010>.
- Palkova Z, Vachova L. 2016. Yeast cell differentiation: lessons from pathogenic and non-pathogenic yeasts. *Semin Cell Dev Biol* 57:110–119. <https://doi.org/10.1016/j.semcdb.2016.04.006>.
- Gancedo JM. 2001. Control of pseudohyphae formation in *Saccharomyces cerevisiae*. *FEMS Microbiol Rev* 25:107–123. <https://doi.org/10.1111/j.1574-6976.2001.tb00573.x>.
- Berman J, Sudbery PE. 2002. *Candida albicans*: a molecular revolution built on lessons from budding yeast. *Nat Rev Genet* 3:918–930. <https://doi.org/10.1038/nrg948>.
- Casperson GF, Walker N, Bourne HR. 1985. Isolation of the gene encoding adenylate cyclase in *Saccharomyces cerevisiae*. *Proc Natl Acad Sci U S A* 82:5060–5063. <https://doi.org/10.1073/pnas.82.15.5060>.
- Rocha CR, Schroppel K, Marcus D, Marciel A, Dignard D, Taylor BN, Thomas DY, Whiteway M, Leberer E. 2001. Signaling through adenylyl cyclase is essential for hyphal growth and virulence in the pathogenic fungus *Candida albicans*. *Mol Biol Cell* 12:3631–3643. <https://doi.org/10.1091/mbc.12.11.3631>.
- Hogan DA, Sundstrom P. 2009. The Ras/cAMP/PKA signaling pathway and virulence in *Candida albicans*. *Future Microbiol* 4:1263–1270. <https://doi.org/10.2217/fmb.09.106>.
- Biswas S, Van Dijk P, Datta A. 2007. Environmental sensing and signal transduction pathways regulating morphopathogenic determinants of *Candida albicans*. *Microbiol Mol Biol Rev* 71:348–376. <https://doi.org/10.1128/MMBR.00009-06>.
- Sheu YJ, Barral Y, Snyder M. 2000. Polarized growth controls cell shape and bipolar bud site selection in *Saccharomyces cerevisiae*. *Mol Cell Biol* 20:5235–5247. <https://doi.org/10.1128/MCB.20.14.5235-5247.2000>.
- Goehring AS, Mitchell DA, Tong AH, Keniry ME, Boone C, Sprague GF, Jr. 2003. Synthetic lethal analysis implicates Ste20p, a p21-activated protein kinase, in polarisome activation. *Mol Biol Cell* 14:1501–1516. <https://doi.org/10.1091/mbc.e02-06-0348>.
- Westfall PJ, Ballon DR, Thorner J. 2004. When the stress of your environment makes you go HOG wild. *Science* 306:1511–1512. <https://doi.org/10.1126/science.1104879>.
- Alonso-Monge R, Navarro-Garcia F, Roman E, Negredo AI, Eisman B, Nombela C, Pla J. 2003. The Hog1 mitogen-activated protein kinase is essential in the oxidative stress response and chlamydospore formation in *Candida albicans*. *Eukaryot Cell* 2:351–361. <https://doi.org/10.1128/EC.2.2.351-361.2003>.
- Barth G, Gaillardin C. 1997. Physiology and genetics of the dimorphic fungus *Yarrowia lipolytica*. *FEMS Microbiol Rev* 19:219–237. <https://doi.org/10.1111/j.1574-6976.1997.tb00299.x>.
- Morin M, Monteoliva L, Insenser M, Gil C, Dominguez A. 2007. Proteomic analysis reveals metabolic changes during yeast to hypha transition in *Yarrowia lipolytica*. *J Mass Spectrom* 42:1453–1462. <https://doi.org/10.1002/jms.1284>.

17. Morales-Vargas AT, Domínguez A, Ruiz-Herrera J. 2012. Identification of dimorphism-involved genes of *Yarrowia lipolytica* by means of microarray analysis. *Res Microbiol* 163:378–387. <https://doi.org/10.1016/j.resmic.2012.03.002>.
18. Martínez-Vázquez A, González-Hernández A, Domínguez A, Rachubinski R, Riquelme M, Cuellar-Mata P, Guzmán JC. 2013. Identification of the transcription factor Znc1p, which regulates the yeast-to-hypha transition in the dimorphic yeast *Yarrowia lipolytica*. *PLoS One* 8:e66790. <https://doi.org/10.1371/journal.pone.0066790>.
19. Zhao XF, Li M, Li YQ, Chen XD, Gao XD. 2013. The TEA/ATTS transcription factor YITec1p represses the yeast-to-hypha transition in the dimorphic yeast *Yarrowia lipolytica*. *FEMS Yeast Res* 13:50–61. <https://doi.org/10.1111/j.1567-1364.2012.12008.x>.
20. Torres-Guzmán JC, Domínguez A. 1997. HOY1, a homeo gene required for hyphal formation in *Yarrowia lipolytica*. *Mol Cell Biol* 17:6283–6293. <https://doi.org/10.1128/MCB.17.11.6283>.
21. González-López CI, Szabo R, Blanchin-Roland S, Gaillardin C. 2002. Genetic control of extracellular protease synthesis in the yeast *Yarrowia lipolytica*. *Genetics* 160:417–427.
22. Liang SH, Wu H, Wang RR, Wang Q, Shu T, Gao XD. 2017. The TORC1-Sch9-Rim15 signaling pathway represses yeast-to-hypha transition in response to glycerol availability in the oleaginous yeast *Yarrowia lipolytica*. *Mol Microbiol* 104:553–567. <https://doi.org/10.1111/mmi.13645>.
23. Hurtado CA, Rachubinski RA. 1999. MHY1 encodes a C2H2-type zinc finger protein that promotes dimorphic transition in the yeast *Yarrowia lipolytica*. *J Bacteriol* 181:3051–3057.
24. Li M, Li YQ, Zhao XF, Gao XD. 2014. Roles of the three Ras proteins in the regulation of dimorphic transition in the yeast *Yarrowia lipolytica*. *FEMS Yeast Res* 14:451–463. <https://doi.org/10.1111/1567-1364.12129>.
25. Zhang H, Liu Q, Cao Y, Feng X, Zheng Y, Zou H, Liu H, Yang J, Xian M. 2014. Microbial production of sabinene—a new terpene-based precursor of advanced biofuel. *Microb Cell Fact* 13:20. <https://doi.org/10.1186/1475-2859-13-20>.
26. Kramara J, Willcox S, Gunisova S, Kinsky S, Nosek J, Griffith JD, Tomaska L. 2010. Tay1 protein, a novel telomere binding factor from *Yarrowia lipolytica*. *J Biol Chem* 285:38078–38092. <https://doi.org/10.1074/jbc.M110.127605>.
27. Koren S, Walenz BP, Berlin K, Miller JR, Bergman NH, Phillippy AM. 2017. Canu: scalable and accurate long-read assembly via adaptive k-mer weighting and repeat separation. *Genome Res* 27:722–736. <https://doi.org/10.1101/gr.215087.116>.
28. van Heerikhuizen H, Ykema A, Klootwijk J, Gaillardin C, Ballas C, Fournier P. 1985. Heterogeneity in the ribosomal RNA genes of the yeast *Yarrowia lipolytica*; cloning and analysis of two size classes of repeats. *Gene* 39:213–222. [https://doi.org/10.1016/0378-1119\(85\)90315-4](https://doi.org/10.1016/0378-1119(85)90315-4).
29. Louis EJ, Naumova ES, Lee A, Naumov G, Haber JE. 1994. The chromosome end in yeast: its mosaic nature and influence on recombinational dynamics. *Genetics* 136:789–802.
30. Mefford HC, Trask BJ. 2002. The complex structure and dynamic evolution of human subtelomeres. *Nat Rev Genet* 3:91–102. <https://doi.org/10.1038/nrg727>.
31. Mathelier A, Fornes O, Arenillas DJ, Chen CY, Denay G, Lee J, Shi W, Shyr C, Tan G, Worsley-Hunt R, Zhang AW, Parcy F, Lenhard B, Sandelin A, Wasserman WW. 2016. JASPAR 2016: a major expansion and update of the open-access database of transcription factor binding profiles. *Nucleic Acids Res* 44:D110–D115. <https://doi.org/10.1093/nar/gkv1176>.
32. Dujon B, Sherman D, Fischer G, Durrans P, Casaregola S, Lafontaine I, De Montigny J, Marck C, Neuvéglise C, Talla E, Goffard N, Frangeul L, Aigle M, Anthouard V, Babour A, Barbe V, Barnay S, Blanchin S, Beckerich J-M, Beyne E, Bleykasten C, Boisramé A, Boyer J, Cattolico L, Confanioli F, De Daruvar A, Despons L, Fabre E, Fairhead C, Ferry-Dumazet H, Groppi A, Hantraye F, Hennequin C, Jauniaux N, Joyet P, Kachouri R, Kerrest A, Koszul R, Lemaire M, Lesur I, Ma L, Muller H, Nicaud J-M, Nikolski M, Oztas S, Ozier-Kalogeropoulos O, Pellenz S, Potier S, Richard G-F, Straub M-L, Suleau A, et al. 2004. Genome evolution in yeasts. *Nature* 430:35–44. <https://doi.org/10.1038/nature02579>.
33. Taylor IA, McIntosh PB, Pala P, Treiber MK, Howell S, Lane AN, Smerdon SJ. 2000. Characterization of the DNA-binding domains from the yeast cell-cycle transcription factors Mbp1 and Swi4. *Biochemistry* 39:3943–3954. <https://doi.org/10.1021/bi992212i>.
34. Wolfe KH. 2015. Origin of the yeast whole-genome duplication. *PLoS Biol* 13:e1002221. <https://doi.org/10.1371/journal.pbio.1002221>.
35. Koch C, Moll T, Neuberg M, Ahorn H, Nasmyth K. 1993. A role for the transcription factors Mbp1 and Swi4 in progression from G1 to S phase. *Science* 261:1551–1557. <https://doi.org/10.1126/science.8372350>.
36. Posas F, Wurgler-Murphy SM, Maeda T, Witten EA, Thai TC, Saito H. 1996. Yeast HOG1 MAP kinase cascade is regulated by a multistep phosphorylation mechanism in the SLN1-YPD1-SSK1 “two-component” osmosensor. *Cell* 86:865–875. [https://doi.org/10.1016/S0092-8674\(00\)80162-2](https://doi.org/10.1016/S0092-8674(00)80162-2).
37. O'Rourke SM, Herskowitz I, O'Shea EK. 2002. Yeast go the whole HOG for the hyperosmotic response. *Trends Genet* 18:405–412. [https://doi.org/10.1016/S0168-9525\(02\)02723-3](https://doi.org/10.1016/S0168-9525(02)02723-3).
38. Ota IM, Varshavsky A. 1993. A yeast protein similar to bacterial two-component regulators. *Science* 262:566–569. <https://doi.org/10.1126/science.8211183>.
39. Nagahashi S, Mio T, Ono N, Yamada-Okabe T, Arisawa M, Bussey H, Yamada-Okabe H. 1998. Isolation of CaSLN1 and CaNIK1, the genes for osmosensing histidine kinase homologues, from the pathogenic fungus *Candida albicans*. *Microbiology* 144:425–432. <https://doi.org/10.1099/00221287-144-2-425>.
40. Calera JA, Choi GH, Calderone RA. 1998. Identification of a putative histidine kinase two-component phosphorelay gene (CaHK1) in *Candida albicans*. *Yeast* 14:665–674. [https://doi.org/10.1002/\(SICI\)1097-0061\(199805\)14:7<665::AID-YEA246>3.0.CO;2-#](https://doi.org/10.1002/(SICI)1097-0061(199805)14:7<665::AID-YEA246>3.0.CO;2-#).
41. Yamada-Okabe T, Mio T, Ono N, Kashima Y, Matsui M, Arisawa M, Yamada-Okabe H. 1999. Roles of three histidine kinase genes in hyphal development and virulence of the pathogenic fungus *Candida albicans*. *J Bacteriol* 181:7243–7247.
42. Aravind L, Ponting CP. 1999. The cytoplasmic helical linker domain of receptor histidine kinase and methyl-accepting proteins is common to many prokaryotic signalling proteins. *FEMS Microbiol Lett* 176:111–116. <https://doi.org/10.1111/j.1574-6968.1999.tb13650.x>.
43. Avenot H, Simoneau P, Iacomini-Vasilescu B, Bataillé-Simoneau N. 2005. Characterization of mutations in the two-component histidine kinase gene AbNIK1 from *Alternaria brassicicola* that confer high dicarboximide and phenylpyrrole resistance. *Curr Genet* 47:234–243. <https://doi.org/10.1007/s00294-005-0568-2>.
44. Buschart A, Gremmer K, El-Mowafy M, van den Heuvel J, Mueller PP, Bilitewski U. 2012. A novel functional assay for fungal histidine kinases group III reveals the role of HAMP domains for fungicide sensitivity. *J Biotechnol* 157:268–277. <https://doi.org/10.1016/j.jbiotec.2011.09.017>.
45. Ochiai N, Fujimura M, Motoyama T, Ichiishi A, Usami R, Horikoshi K, Yamaguchi I. 2001. Characterization of mutations in the two-component histidine kinase gene that confer fludioxonil resistance and osmotic sensitivity in the os-1 mutants of *Neurospora crassa*. *Pest Manag Sci* 57:437–442. <https://doi.org/10.1002/ps.302>.
46. Hagiwara D, Matsubayashi Y, Marui J, Furukawa K, Yamashino T, Kanamaru K, Kato M, Abe K, Kobayashi T, Mizuno T. 2007. Characterization of the Nika histidine kinase implicated in the phosphorelay signal transduction of *Aspergillus nidulans*, with special reference to fungicide responses. *Biosci Biotechnol Biochem* 71:844–847. <https://doi.org/10.1271/bbb.70051>.
47. Raivio TL, Silhavy TJ. 1997. Transduction of envelope stress in *Escherichia coli* by the Cpx two-component system. *J Bacteriol* 179:7724–7733. <https://doi.org/10.1128/jb.179.24.7724-7733.1997>.
48. Park H, Inouye M. 1997. Mutational analysis of the linker region of EnvZ, an osmosensor in *Escherichia coli*. *J Bacteriol* 179:4382–4390. <https://doi.org/10.1128/jb.179.13.4382-4390.1997>.
49. Collins LA, Egan SM, Stewart V. 1992. Mutational analysis reveals functional similarity between NARX, a nitrate sensor in *Escherichia coli* K-12, and the methyl-accepting chemotaxis proteins. *J Bacteriol* 174:3667–3675. <https://doi.org/10.1128/jb.174.11.3667-3675.1992>.
50. Nelson B, Kurischko C, Horecka J, Mody M, Nair P, Pratt L, Zougman A, McBroom LD, Hughes TR, Boone C, Luca FC. 2003. RAM: a conserved signaling network that regulates Ace2p transcriptional activity and polarized morphogenesis. *Mol Biol Cell* 14:3782–3803. <https://doi.org/10.1091/mbc.e03-01-0018>.
51. Lorberg A, Schmitz HP, Jacoby JJ, Heinisch JJ. 2001. Lrg1p functions as a putative GTPase-activating protein in the Pkc1p-mediated cell integrity pathway in *Saccharomyces cerevisiae*. *Mol Genet Genomics* 266:514–526. <https://doi.org/10.1007/s004380100580>.
52. Sia RA, Herald HA, Lew DJ. 1996. Cdc28 tyrosine phosphorylation and the morphogenesis checkpoint in budding yeast. *Mol Biol Cell* 7:1657–1666. <https://doi.org/10.1091/mbc.7.11.1657>.
53. Kuranda MJ, Robbins PW. 1991. Chitinase is required for cell separation during growth of *Saccharomyces cerevisiae*. *J Biol Chem* 266:19758–19767.

54. Martinez-Pastor MT, Marchler G, Schuller C, Marchler-Bauer A, Ruis H, Estruch F. 1996. The *Saccharomyces cerevisiae* zinc finger proteins Msn2p and Msn4p are required for transcriptional induction through the stress response element (STRE). *EMBO J* 15:2227–2235. <https://doi.org/10.1002/j.1460-2075.1996.tb00576.x>.
55. Pomraning KR, Bredeweg EL, Baker SE. 2017. Regulation of nitrogen metabolism by GATA zinc finger transcription factors in *Yarrowia lipolytica*. *mSphere* 2:e00038-17. <https://doi.org/10.1128/mSphere.00038-17>.
56. Grenetier S, Bouchoux C, Goguel V. 2006. CTD kinase I is required for the integrity of the rDNA tandem array. *Nucleic Acids Res* 34:4996–5006. <https://doi.org/10.1093/nar/gkl493>.
57. Salim D, Bradford WD, Freeland A, Cady G, Wang J, Pruitt SC, Gerton JL. 2017. DNA replication stress restricts ribosomal DNA copy number. *PLoS Genet* 13:e1007006. <https://doi.org/10.1371/journal.pgen.1007006>.
58. Russell PJ, Rodland KD. 1986. Magnification of rRNA gene number in a *Neurospora crassa* strain with a partial deletion of the nucleolus organizer. *Chromosoma* 93:337–340. <https://doi.org/10.1007/BF00327592>.
59. Rodland KD, Russell PJ. 1983. Segregation of heterogeneous rDNA segments during demagnification of a *Neurospora crassa* strain possessing a double nucleolar organizer. *Curr Genet* 7:379–384. <https://doi.org/10.1007/BF00445878>.
60. Rustchenko EP, Curran TM, Sherman F. 1993. Variations in the number of ribosomal DNA units in morphological mutants and normal strains of *Candida albicans* and in normal strains of *Saccharomyces cerevisiae*. *J Bacteriol* 175:7189–7199. <https://doi.org/10.1128/jb.175.22.7189-7199.1993>.
61. Schmitt AP, McEntee K. 1996. Msn2p, a zinc finger DNA-binding protein, is the transcriptional activator of the multistress response in *Saccharomyces cerevisiae*. *Proc Natl Acad Sci U S A* 93:5777–5782. <https://doi.org/10.1073/pnas.93.12.5777>.
62. Sunnaker M, Zamora-Sillero E, Dechant R, Ludwig C, Busetto AG, Wagner A, Stelling J. 2013. Automatic generation of predictive dynamic models reveals nuclear phosphorylation as the key Msn2 control mechanism. *Sci Signal* 6:ra41. <https://doi.org/10.1126/scisignal.2003621>.
63. Görner W, Durchschlag E, Martinez-Pastor MT, Estruch F, Ammerer G, Hamilton B, Ruis H, Schüller C. 1998. Nuclear localization of the C2H2 zinc finger protein Msn2p is regulated by stress and protein kinase A activity. *Genes Dev* 12:586–597. <https://doi.org/10.1101/gad.12.4.586>.
64. Garreau H, Hasan RN, Renault G, Estruch F, Boy-Marcotte E, Jacquet M. 2000. Hyperphosphorylation of Msn2p and Msn4p in response to heat shock and the diauxic shift is inhibited by cAMP in *Saccharomyces cerevisiae*. *Microbiology* 146:2113–2120. <https://doi.org/10.1099/00221287-146-9-2113>.
65. Estruch F. 2000. Stress-controlled transcription factors, stress-induced genes and stress tolerance in budding yeast. *FEMS Microbiol Rev* 24: 469–486. <https://doi.org/10.1111/j.1574-6976.2000.tb00551.x>.
66. Bean JM, Siggia ED, Cross FR. 2005. High functional overlap between MluI cell-cycle box binding factor and Swi4/6 cell-cycle box binding factor in the G1/S transcriptional program in *Saccharomyces cerevisiae*. *Genetics* 171:49–61. <https://doi.org/10.1534/genetics.105.044560>.
67. Bahler J. 2005. Cell-cycle control of gene expression in budding and fission yeast. *Annu Rev Genet* 39:69–94. <https://doi.org/10.1146/annurev.genet.39.110304.095808>.
68. El-Mowafy M, Bahgat MM, Bililewski U. 2013. Deletion of the HAMP domains from the histidine kinase CaNik1p of *Candida albicans* or treatment with fungicides activates the MAP kinase Hog1p in *S. cerevisiae* transformants. *BMC Microbiol* 13:209. <https://doi.org/10.1186/1471-2180-13-209>.
69. Defosse TA, Sharma A, Mondal AK, Duge de Bernonville T, Latge JP, Calderone R, Giglioli-Guivarc'h N, Courdavault V, Clastre M, Papon N. 2015. Hybrid histidine kinases in pathogenic fungi. *Mol Microbiol* 95: 914–924. <https://doi.org/10.1111/mmi.12911>.
70. Foureau E, Clastre M, Obando Montoya EJ, Besseau S, Oudin A, Glévarec G, Simkin AJ, Crèche J, Atehortua L, Giglioli-Guivarc'h N, Courdavault V, Papon N. 2014. Subcellular localization of the histidine kinase receptors Sln1p, Nik1p and Chk1p in the yeast CTG clade species *Candida guilliermondii*. *Fungal Genet Biol* 65:25–36. <https://doi.org/10.1016/j.fgb.2014.01.007>.
71. Winston F. 2008. EMS and UV mutagenesis in yeast. *Curr Protoc Mol Biol* Chapter 13:Unit 13.3B. <https://doi.org/10.1002/0471142727.mb1303bs82>.
72. Verdunyn C, Postma E, Scheffers WA, Van Dijken JP. 1992. Effect of benzoic acid on metabolic fluxes in yeasts: a continuous-culture study on the regulation of respiration and alcoholic fermentation. *Yeast* 8:501–517. <https://doi.org/10.1002/yea.320080703>.
73. Grigoriev IV, Nikitin R, Haridas S, Kuo A, Ohm R, Otilar R, Riley R, Salamov A, Zhao X, Korzeniewski F, Smirnova T, Nordberg H, Dubchak I, Shabalov I. 2014. MycoCosm portal: gearing up for 1000 fungal genomes. *Nucleic Acids Res* 42:D699–D704. <https://doi.org/10.1093/nar/gkt1183>.
74. Grabherr MG, Haas BJ, Yassour M, Levin JZ, Thompson DA, Amit I, Adiconis X, Fan L, Raychowdhury R, Zeng Q, Chen Z, Mauceli E, Hacohen N, Gnirke A, Rhind N, di Palma F, Birren BW, Nusbaum C, Lindblad-Toh K, Friedman N, Regev A. 2011. Full-length transcriptome assembly from RNA-Seq data without a reference genome. *Nat Biotechnol* 29:644–652. <https://doi.org/10.1038/nbt.1883>.
75. Li H, Durbin R. 2009. Fast and accurate short read alignment with Burrows-Wheeler transform. *Bioinformatics* 25:1754–1760. <https://doi.org/10.1093/bioinformatics/btp324>.
76. Langmead B, Salzberg SL. 2012. Fast gapped-read alignment with Bowtie 2. *Nat Methods* 9:357–359. <https://doi.org/10.1038/nmeth.1923>.
77. Thorvaldsdottir H, Robinson JT, Mesirov JP. 2013. Integrative Genomics Viewer (IGV): high-performance genomics data visualization and exploration. *Brief Bioinform* 14:178–192. <https://doi.org/10.1093/bib/bbs017>.
78. Li H. 2011. A statistical framework for SNP calling, mutation discovery, association mapping and population genetical parameter estimation from sequencing data. *Bioinformatics* 27:2987–2993. <https://doi.org/10.1093/bioinformatics/btr509>.
79. Ye K, Schulz MH, Long Q, Apweiler R, Ning Z. 2009. Pindel: a pattern growth approach to detect break points of large deletions and medium sized insertions from paired-end short reads. *Bioinformatics* 25: 2865–2871. <https://doi.org/10.1093/bioinformatics/btp394>.
80. Chen K, Wallis JW, McLellan MD, Larson DE, Kalicki JM, Pohl CS, McGrath SD, Wendt MC, Zhang Q, Locke DP, Shi X, Fulton RS, Ley TJ, Wilson RK, Ding L, Mardis ER. 2009. BreakDancer: an algorithm for high-resolution mapping of genomic structural variation. *Nat Methods* 6:677–681. <https://doi.org/10.1038/nmeth.1363>.
81. Abyzov A, Urban AE, Snyder M, Gerstein M. 2011. CNVnator: an approach to discover, genotype, and characterize typical and atypical CNVs from family and population genome sequencing. *Genome Res* 21:974–984. <https://doi.org/10.1101/gr.114876.110>.
82. Cingolani P, Platts A, Wang LL, Coon M, Nguyen T, Wang L, Land SJ, Lu X, Ruden DM. 2012. A program for annotating and predicting the effects of single nucleotide polymorphisms, SnpEff: SNPs in the genome of *Drosophila melanogaster* strain w1118; iso-2; iso-3. *Fly (Austin)* 6:80–92. <https://doi.org/10.4161/fly.19695>.
83. Gietz RD, Woods RA. 2002. Transformation of yeast by lithium acetate/single-stranded carrier DNA/polyethylene glycol method. *Methods Enzymol* 350:87–96. [https://doi.org/10.1016/S0076-6879\(02\)50957-5](https://doi.org/10.1016/S0076-6879(02)50957-5).
84. Anders S, Pyl PT, Huber W. 2015. HTSeq—a Python framework to work with high-throughput sequencing data. *Bioinformatics* 31:166–169. <https://doi.org/10.1093/bioinformatics/btu638>.
85. Law CW, Chen Y, Shi W, Smyth GK. 2014. voom: precision weights unlock linear model analysis tools for RNA-seq read counts. *Genome Biol* 15: R29. <https://doi.org/10.1186/gb-2014-15-2-r29>.
86. Pathan M, Keerthikumar S, Ang CS, Gangoda L, Quek CY, Williamson NA, Mouradov D, Sieber OM, Simpson RJ, Salim A, Bacic A, Hill AF, Stroud DA, Ryan MT, Agbinya JJ, Mariadason JM, Burgess AW, Mathivanan S. 2015. FunRich: an open access standalone functional enrichment and interaction network analysis tool. *Proteomics* 15:2597–2601. <https://doi.org/10.1002/pmic.201400515>.
87. Bailey TL. 2011. DREME: motif discovery in transcription factor ChIP-seq data. *Bioinformatics* 27:1653–1659. <https://doi.org/10.1093/bioinformatics/btr261>.
88. Gupta S, Stamatoyannopoulos JA, Bailey TL, Noble WS. 2007. Quantifying similarity between motifs. *Genome Biol* 8:R24. <https://doi.org/10.1186/gb-2007-8-2-r24>.
89. Schneider CA, Rasband WS, Eliceiri KW. 2012. NIH Image to ImageJ: 25 years of image analysis. *Nat Methods* 9:671–675. <https://doi.org/10.1038/nmeth.2089>.
90. Finn RD, Attwood TK, Babbitt PC, Bateman A, Bork P, Bridge AJ, Chang HY, Dosztanyi Z, El-Gebali S, Fraser M, Gough J, Haft D, Holliday GL, Huang H, Huang X, Letunic I, Lopez R, Lu S, Marchler-Bauer A, Mi H, Mistry J, Natale DA, Necci M, Nuka G, Orengo CA, Park Y, Pesseat S, Piovesan D, Potter SC, Rawlings ND, Redaschi N, Richardson L, Rivoire C, Sangrador-Vegas A, Sigrist C, Sillitoe I, Smithers B, Squizzato S, Sutton G, Thanki N, Thomas PD, Tosatto SC, Wu CH, Xenarios I, Yeh LS, Young SY, Mitchell AL. 2017. InterPro in 2017—beyond protein family and domain annotations. *Nucleic Acids Res* 45:D190–D199. <https://doi.org/10.1093/nar/gkw1107>.